Supporting Online Material for

Atmospheric Carbon Dioxide Concentration Across the Mid-Pleistocene Transition

Bärbel Hönisch, N. Gary Hemming, David Archer, Mark Siddall, Jerry F. McManus

Published 19 June 2009, *Science* **324**, 1551 (2009)
DOI: 10.1126/science.1171477

This PDF file includes:

Atmospheric Carbon Dioxide Concentration over the Mid-Pleistocene Transition

Bärbel Hönisch, N. Gary Hemming, David Archer, Mark Siddall

and Jerry F. McManus

Supporting online material

Materials and Methods

1. Foraminifer samples. The shallow water depth of ODP 668B is beneficial to the preservation of planktic foraminifer shells, as the $\delta^{11}B$ signal recorded in *G. sacculifer* has been shown to be prone to dissolution (*1*). $\delta^{18}O$ was measured in shells of the surface dwelling *Globigerinoides ruber* (white, 250-300 μm size fraction) at a 3-7 cm resolution. Complementary shell weight measurements on the ultrasonically cleaned *G. ruber* shells allowed us to avoid selecting partially dissolved shells for boron isotope analysis. In addition, *Globigerinoides sacculifer* shells were selected from the largest size fraction (515-865 μm), as larger shells are less susceptible to dissolution and empirical calibration has shown that their $\delta^{11}B$ reflects surface seawater pH (*1*). Boron isotope measurements were complemented by Mg/Ca in 80 small (250-300 μm) shells of *G. ruber* (white), which inhabits the same depth range as large *G. sacculifer* (*2*).

2. pH reconstruction and empirical calibration. Boric acid [$B(OH)_3$] and borate [$B(OH)_4^-$] are the two dominant species of dissolved boron in seawater. At low *p*H (<7) virtually all boron is present in the form of boric acid, whereas at high *p*H (>10) boron exists predominately in the form of borate. The stable isotope ^{11}B is enriched in $B(OH)_3$

compared to $B(OH)_4^-$, with a constant isotopic fractionation between the two boron species (*3, 4*). Consequently, as the relative concentration of the dissolved species changes with pH, so does their isotopic composition. Empirical calibration with live cultured planktic foraminifers and corals has shown that the isotopic composition of biogenic carbonates falls close to the isotopic composition of borate in seawater (*5-8*), although the empirical $\delta^{11}B_{carbonate}$/pH relationship is not as steep as predicted by the isotopic fractionation between borate and boric acid in seawater (*3*). Presently the reason for this discrepancy remains unresolved. However, it is clear that the use of empirical calibration curves yields high-quality results, as demonstrated by the quantitative replication of the Vostok pCO_2 record from boron isotopes in the planktic foraminifer *Globigerinoides sacculifer* (*9*).

Data presented in this study were measured on two different Thermal Ionization Mass Spectromters (TIMS), a 15-cm radius of curvature NBS-design instrument at SUNY Stony Brook and a Thermo Scientific TRITON at the Lamont-Doherty Earth Observatory (LDEO). Although chemical pretreatment of both sample sets was identical and exclusively completed at LDEO, $\delta^{11}B$ of *G. sacculifer* measured on the TRITON was lower than data measured on the NBS design TIMS at SUNY Stony Brook (*1, 9*). An interlaboratory comparison of five modern and fossil *G. sacculifer* samples measured at LDEO on the TRITON and at SUNY Stony Brook on the NBS instrument, revealed a consistent offset of -1.1‰ on the TRITON that is not accounted for by standardization against NBS 951. The only difference other than the instrument is the use of boron free seawater (BFSW) at LDEO, which was added both to the samples and the boric acid standard. Analyses at SUNY Stony Brook were typically done without addition of BFSW

but occasional comparisons did not reveal a difference between samples measured with or without BFSW. We do not know what causes this instrument difference but we found that poor ionization at 980°C and excessive fractionation at temperatures >1020°C prohibit the analysis of foraminifer samples without boron free seawater on the TRITON. The observed offset raises additional questions regarding the shape of the calibration curve used for translating $\delta^{11}B$ data measured at LDEO into pH. All published calibration curves have been measured on the NBS instrument at SUNY Stony Brook and their shape and inflection point does not match the isotopic composition of dissolved borate in seawater (*3, 10*). Although sound reconstructions can be achieved as long as the appropriate empirical calibrations are applied, a calibration curve measured on the TRITON could potentially differ from a calibration curve established on the NBS machine. We tested this on a pair of cultured *Orbulina universa* shell samples, which were grown at ambient and elevated seawater pH (7.95 and 8.35, respectively) in July/August 2008 on Catalina Island, California. The culture procedures were identical to (*7*) and the measured $\delta^{11}B$ of those two samples (18.35 and 20.95‰, respectively) confirms the earlier calibration by (*7*), demonstrating that the shape and inflection point of published calibrations is also applicable to samples measured on a TRITON. Remarkably, no offset exists between *O. universa* samples measured at LDEO (with BFSW) and at SUNY Stony Brook (with and without BFSW). We hope our (G. Foster - U. Bristol, M. McCulloch & S. Eggins - ANU, J. Gaillardet – IPGP, and B. Hönisch - LDEO) ongoing interlaboratory and instrument (TIMS and ICP-MS) comparison experiment will improve our understanding of instrument and matrix effects on boron isotope analyses.

$\delta^{11}B$ data were translated into pH estimates using the following equation:

$$pH = pK_B - \log(-(\delta^{11}B_{sw} - \delta^{11}B_c - a) / (\delta^{11}B_{sw} - \alpha^* (\delta^{11}B_c + a) - \varepsilon)),$$

where pK_B is the equilibrium constant for the boric acid/borate system for a given temperature and salinity (*11*), $\delta^{11}B_{sw}$=39.5‰, $\delta^{11}B_c$ is the isotopic composition of the measured carbonate, and ε = (fractionation factor a-1)*1000 is the temperature dependent fractionation after (*4*). The constant 'a' is the fixed offset between the theoretical borate and empirical $\delta^{11}B$/pH-calibration curve for *G. sacculifer*, where samples measured on the NBS instrument were corrected by -3.1‰ (*8, 10*) and samples measured on the TRITON were corrected by -4.2‰. It should be noted that samples measured at SUNY Stony Brook and LDEO are randomly distributed over the record presented here (Table S1) and a systematic bias can thus be excluded. Temperature and salinity values used for these calculations are given in Table S1 and estimations are described in the following.

3. Mg/Ca-SST estimates. Shells were crushed and then cleaned using a multi-step process including repeated rinses in ultrapure water and methanol, hot reducing and oxidizing treatments. Samples were then dissolved in 0.075 N HNO_3 and analyzed in duplicate on a JY Panorama ICP-AES (ion-coupled plasma atomic emission spectrometry) at the Lamont-Doherty Earth Observatory. Mg/Ca ratios were translated to sea surface temperature (SST) using a *G. ruber* depth-corrected coretop calibration for the tropical Atlantic (i.e., Mg/Ca=0.38 exp 0.09 * (SST-0.61*core depth km), *12*). A recent culture calibration identified a small salinity effect on Mg/Ca in *G. ruber* (*13*),

which suggests glacial SST estimates at ODP site 668B may be overestimated by up to 1°C for a 3% higher glacial salinity (i.e. -125 m sea level). To evaluate whether this temperature difference propagates into a significant change on the PCO_2 estimate, we recalculated the constant alkalinity scenario with these corrected temperature estimates and found the result to be indistinguishable from the scenario using uncorrected SST estimates (Figure S1).

4. Salinity and alkalinity estimates. The glacial/interglacial variability of salinity and alkalinity were calculated as a function of global sea-level, as determined by (*14*). The sea-level record, like our age model, is based on LR04, so that age differences can be neglected. Based on the sea-level record, local salinity at a time t can be approximated as

S_t = 35.7‰ + meters of sea-level below modern/3800 m * 34.8‰ (Equation 1),

where 35.7‰ is the modern salinity at the core site, 3800 m is the average ocean depth and 34.8‰ is the average ocean salinity.

Several proxies for reconstructing [$CO_3^{=}$] have been suggested in the past decade, including U/Ca, foraminiferal shell weight and B/Ca, but none are applicable to our study. The residence time of U in seawater is too short for the time period studied here (*15*), planktic foraminiferal shell weights are equally controlled by dissolution and calcification (*16, 17*) and it is not yet clear whether B/Ca actually reflects [$CO_3^{=}$] (*18*) or pH (*19*). We therefore reconstructed alkalinity according to two scenarios:

(1) The "constant alkalinity scenario" assumes that total alkalinity (A_T) remained constant in the past and alkalinity can thus be estimated from the modern alkalinity/salinity relationship at the core site (*9*):

$A_T = 65.62 * S + 22.84$ ($R^2=0.57$) (Equation 2).

(2) Our "varying alkalinity scenario" follows (*20*), who estimated past average ocean alkalinity amongst others from terrestrial silicate weathering rates, where independent records of Sr, Hf and Os isotopes provide consistent evidence for increasing exposure of crystalline bedrock of the Canadian Shield in response to the waxing and waning of the northern hemisphere ice sheet. The modeled alkalinity varies significantly, by up to 10.7-12.5% over the course of the period studied here, depending on the contribution (4 or 8%, respectively) of weathering the Canadian Shield to total global weathering rates. Because the average alkalinity estimates by (*20*) reflect global values and do not resolve glacial/interglacial periods, we scaled the global alkalinity estimate to the modern alkalinity measured at the core site and adjusted alkalinity similar to the salinity variations in response to sea level changes. In summary, weathering-included alkalinity was calculated as

$A_{T\text{-}t} = 2366\ \mu molkg^{-1} - \text{global } A_{T\text{-}t0} + \text{global } A_{T\text{-}t} * S_t/35.7‰$ (Equation 3),

where 2366 $\mu molkg^{-1}$ is the modern alkalinity observed at the core site, global $A_{T\text{-}t0}$ and global $A_{T\text{-}t}$ are the modern and past values estimated by (*20*), S_t is the salinity estimate

from Equation 1 and 35.7‰ is the modern salinity at the study site. A 5-point running mean was calculated for the 1–kyr resolved alkalinity data (*20*), to account for differences in the age models. The alkalinity estimates are presented in Figure S1.

5. Error propagation. The uncertainty of all PCO_2 estimates presented here is based on the propagated error of the individual uncertainties of pH (±0.23‰ in $\delta^{11}B$ or ±18.1 ppm in PCO_2 on average), temperature (±3% in Mg/Ca or ~±0.77˚C on the temperature estimate or ±5.4 ppm on average), salinity (sea level ±2000 years as determined by (*14*), ±0.06‰ in salinity or ±0.4 ppm on average) and alkalinity (±27 μmol kg^{-1} or ±3.0 ppm on average) on the PCO_2 estimate. The average propagated error for our varying alkalinity scenario is thus ±19.1 μatm and is dominated by the 2σ uncertainty of boron isotope analyses.

6. Validation

Paleoceanographic proxies are often controlled by more than one parameter, and because SST varies significantly on glacial/interglacial (G/I) time scales, that potential control on the pH estimate must be ruled out. A strong linear relationship exists between $\delta^{18}O_c$ and $\delta^{11}B_c$ (R^2=0.83, not shown, and R^2=0.76 for the residual $\delta^{18}O_{sw}$ after removal of the SST contribution to $\delta^{18}O_c$, Fig. S2) but only a weak relationship between $\delta^{11}B_c$ and Mg/Ca-temperatures (R^2=0.34, Fig. S2). The lack of a strong temperature correlation is not surprising, as PCO_2 at this site is in equilibrium with the atmosphere and thus reflects the global pCO_2, whereas SST at the core site likely reflects local temperature. In contrast, the residual $\delta^{18}O_{sw}$ is broadly related to global ice volume, which co-varies with pCO_2.

The weak temperature correlation thus supports the notion that the pH signal described here is not a temperature driven artifact of the boron isotope proxy.

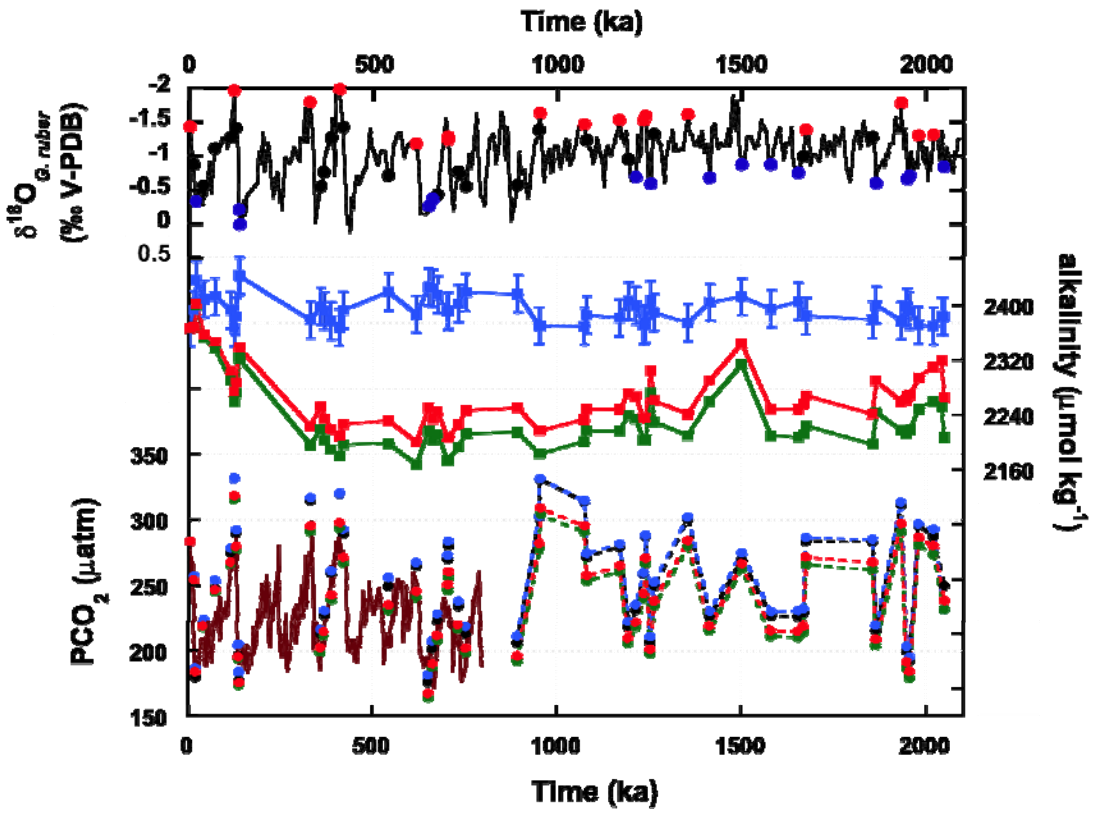

Figure S1. Comparison of various scenarios to estimate PCO_2 from boron isotopes. The planktic oxygen isotope stratigraphy of ODP 668B is shown on the upper panel as a reference. Red, black and blue circles indicate samples analyzed for the PCO_2 reconstruction, where red indicates extreme interglacial samples and blue indicates extreme glacial samples. Black circles are transitional samples, which were not used for averages calculate in Table 1. The middle panel shows theoretical alkalinity estimates to complement the δ^{11}B-pH estimates for calculating PCO_2. Blue squares reflect Scenario 1, where alkalinity remained constant over the past 2.1 Ma and only varied as a function of sea level. Green and red squares in Scenario 2 consider changes in continental weathering, marine $CaCO_3$ production and seafloor dissolution after (*20*). Green squares reflect an estimate where the Canadian Shield modulates 8% of the global weathering rate and red squares reflect our preferred estimate, where the Canadian Shield modulates 4% of global weathering. The lower panel shows the effect of the various alkalinity estimates on PCO_2. Scenario 1 is shown in blue. Black symbols indicate the effect of salinity on the Mg/Ca temperature estimate after (*13*). Red and green symbols reflect Scenario 2, where 4% Canadian Shield weathering (red symbols) results in a slightly better match with the ice core pCO_2 measurements (dark red line) than 8% Canadian Shield weathering (green symbols). The overall difference in the PCO_2 estimates (up to 27 µatm) is small compared to the much larger difference in alkalinity (up to 221 µmol kg^{-1}). All scenarios agree that pre-MPT glacials were characterized by relatively higher PCO_2. But where our preferred weathering scenarios show pre-MPT interglacial PCO_2 similar to interglacials of the past 400 kyr (280 µatm on average), the constant alkalinity scenario suggests systematically higher PCO_2 and average interglacial PCO_2 may have been as high as 296 µatm.

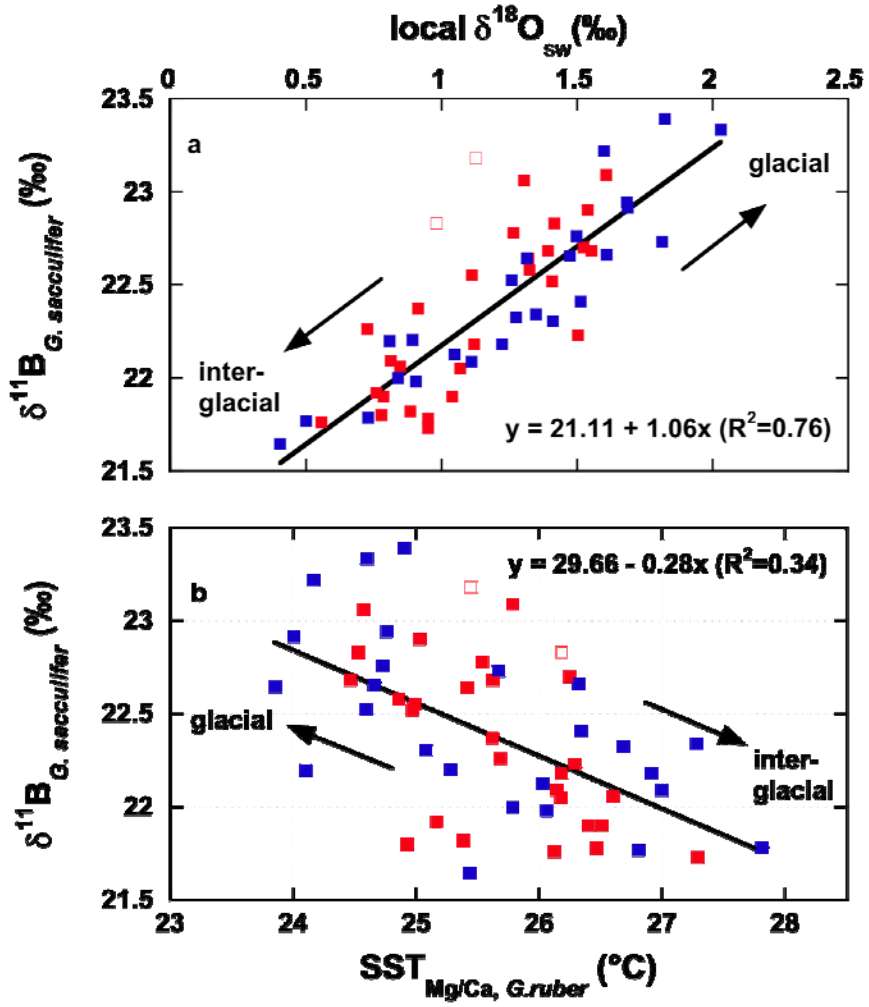

Figure S2. Cross-plots of **(a)** planktic $\delta^{11}B$ vs. residual surface ocean $\delta^{18}O$ and **(b)** $\delta^{11}B$ vs. SST. The SST contribution to the planktic $\delta^{18}O$ has been removed following the empirical equation of (*21*), where T(°C) = 14.9 - 4.80 * (δc-δw). Linear regressions have been calculated for the entire 2.1-Ma data sets. Pre-MPT data are highlighted in red, post-MPT data in blue. Note that the correlation with local $\delta^{18}O_{sw}$ is much stronger than with SST, indicating that temperature merely co-varies with paleo-pH rather than exerts control on the boron isotope proxy. Open symbols identify outliers from the $\delta^{11}B$ vs. $\delta^{18}O_{sw}$ correlation. These data may actually indicate a lead/lag relationship between $\delta^{18}O$ and $\delta^{11}B$, but our temporal resolution does not allow for interpretation of such a pattern. These data have been excluded from both regressions and from Figures 1 and S1.

Table S1. Proxy data, alkalinity and PCO_2 estimates. $\delta^{11}B$ data with an asterisk indicate data measured on the TRITON at LDEO, other data were measured on the NBS instrument at SUNY SB. LDEO data were corrected for a -1.1‰ offset between data measured at LDEO and SUNY SB, see text for details. Oxygen isotopes and Mg/Ca were measured on *G. ruber* (250-300 μm), boron isotopes on large *G. sacculifer* (515-865 μm). Data in brackets are considered outliers, as their $\delta^{11}B$ falls off the general $\delta^{11}B/\delta^{18}O$ correlation (Fig. S1). These data were excluded from Figure 1 and the main text. Mg/Ca was translated to SST using the equation of (*12*), and the salinity correction after (*13*). The constant alkalinity scenario assumes alkalinity changed only according to sea level change. The varying alkalinity scenarios take into account past changes in terrestrial weathering, rate of $CaCO_3$ production and sedimentary dissolution, where 4% and 8% reflect the degree to which the Canadian Shield modulates terrestrial weathering rates (*20*). PCO_2 estimates are based on the various alkalinity and temperature estimates, where the varying alkalinity scenario with 4% modulation of Canadian Shield weathering matches ice core measurements best (Fig. 1A). The PCO_2 uncertainty is similar for all estimates, given here is the specific uncertainty for our preferred "var. alk. 4%" scenario.

ODP 668B core-section, cm	Time (ka)	$\delta^{18}O$ (‰)	$\delta^{11}B$ (‰)	pH (SWS)	pH uncertainty	Mg/Ca (mmol/mol)	SST (°C)	SST sal. corr. (°C)	S (‰)	alkalinity constant ($\mu mol\ kg^{-1}$)	alkalinity varying 4% ($\mu mol\ kg^{-1}$)	alkalinity varying 8% ($\mu mol\ kg^{-1}$)	PCO_2 const. alk. (μatm)	PCO_2 SST sal. corr. (μatm)	PCO_2 var. alk. 4% (μatm)	PCO_2 uncertainty	PCO_2 var. alk. 8% (μatm)
1-1, 2-4	3.6	-1.43	22.00	8.16	0.03	3.34	25.8	25.8	35.7	2366.3	2366.3	2366.3	283.4	283.4	283.4	23.0	283.4
1-1, 2-4			21.94*														
1-1, 25-27	14.6	-0.87	22.41	8.19	0.02	3.51	26.3	26.1	36.1	2392.7	2368.0	2367.6	256.8	253.9	253.9	20.2	253.9
1-1, 25-27			22.54*														
1-1, 33-35	20.4	-0.33	23.22	8.30	0.02	2.88	24.2	23.2	36.8	2436.4	2401.2	2399.7	186.3	179.7	183.4	13.8	183.3
1-1, 70-72	40.8	-0.56	22.65	8.24	0.02	3.01	24.7	24.1	36.4	2408.7	2356.4	2351.9	223.6	218.9	218.4	16.9	218.0
1-1, 105-107	70.6	-1.11	22.20	8.20	0.02	2.87	24.1	23.5	36.4	2412.5	2346.3	2337.6	253.6	247.5	246.3	19.5	245.3
1-2, 25-27	113.6	-1.27	22.12	8.17	0.03	3.41	26.0	25.8	36.1	2392.4	2303.5	2290.1	278.2	275.1	267.3	21.6	265.6
1-2, 39-41	123.2	-1.96	21.78	8.10	0.03	4.00	27.8	27.8	35.7	2366.4	2273.6	2259.4	331.5	331.5	317.8	26.7	315.7
1-2, 49-51	128.1	-1.41	22.09	8.15	0.03	3.72	27.0	26.8	36.0	2383.3	2286.4	2271.8	291.9	289.9	279.3	22.8	277.4
1-2, 70-72	136.8	-0.21	22.91	8.28	0.02	2.84	24.0	23.0	36.9	2443.1	2338.6	2323.1	204.2	195.9	194.9	14.9	193.5
1-2, 74-76	138.6	0.01	23.33	8.31	0.02	3.00	24.6	23.6	36.9	2442.0	2337.3	2320.6	183.6	176.8	175.2	13.2	173.8
2-2, 56-58	329.1	-1.79	21.65	8.12	0.03	3.23	25.4	25.3	35.9	2378.3	2223.7	2196.2	316.5	314.7	294.8	24.6	291.0
2-2, 105-107	358.5	-0.55	22.64	8.25	0.02	2.80	23.9	23.4	36.2	2397.8	2251.9	2218.9	215.8	212.3	201.9	15.6	198.7
2-2, 130-132	366.9	-0.76	22.52	8.23	0.02	3.00	24.6	24.3	36.1	2391.7	2233.7	2202.8	230.3	227.4	214.1	16.7	211.0
2-3, 14-16	386.4	-1.27	22.20	8.19	0.03	3.19	25.3	25.2	35.9	2376.9	2218.8	2189.5	260.7	259.4	242.3	19.4	238.9
2-3, 56-58	409.1	-1.98	21.77	8.11	0.03	3.66	26.8	26.8	35.7	2367.7	2209.4	2180.0	320.0	319.8	297.5	24.9	293.3
2-3, 70-72	418.8	-1.42	21.98	8.15	0.03	3.42	26.1	25.8	36.1	2392.4	2226.6	2196.7	292.5	289.2	271.1	22.2	267.3
2-4, 94-96	541.6	-0.71	22.30	8.20	0.02	3.13	25.1	24.5	36.5	2419.3	2231.6	2198.2	255.9	249.4	234.8	18.6	231.1
2-5, 37-39	616.3	-1.18	22.32	8.18	0.02	3.62	26.7	26.5	36.0	2386.4	2200.7	2167.8	267.0	264.8	244.9	19.7	241.0
2-5, 73-75	651.0	-0.26	23.39	8.31	0.02	3.08	24.9	24.2	36.6	2426.8	2250.3	2216.5	181.1	175.9	166.9	12.6	164.2
2-5, 80-82	662.1	-0.37	22.94	8.27	0.02	3.04	24.8	24.0	36.6	2424.5	2233.6	2203.9	206.8	201.0	189.4	14.5	186.7
2-5, 87-89	675.0	-0.43	22.73	8.23	0.02	3.30	25.7	25.1	36.5	2415.0	2245.3	2211.2	228.1	223.1	211.0	16.4	207.6
2-6, 14-16	702.2	-1.23	22.34	8.17	0.03	3.82	27.3	27.1	36.1	2390.4	2206.4	2173.3	272.6	270.1	250.4	20.2	246.3
2-6, 25-27	703.5	-1.28	22.18	8.16	0.03	3.69	26.9	26.7	36.1	2392.1	2207.1	2174.2	283.4	280.5	260.2	21.1	256.0
2-6, 69-71	731.0	-0.77	22.66	8.22	0.02	3.50	26.3	26.0	36.3	2401.9	2226.4	2193.3	237.8	234.3	219.3	17.2	215.8
2-6, 90-92	752.4	-0.55	22.76	8.25	0.02	3.03	24.7	24.1	36.5	2418.4	2246.5	2213.0	217.9	212.4	201.4	15.6	198.2
3-1, 99-101	891.9	-0.57	22.90*	8.26	0.02	3.12	25.0	24.4	36.5	2416.3	2250.2	2214.5	210.8	205.8	195.3	15.0	192.0
3-2, 39-41	950.0	-1.38	21.90*	8.13	0.03	3.56	26.5	26.5	35.8	2369.6	2217.3	2183.6	302.4	302.0	281.9	23.2	277.3
3-2, 46-48	952.8	-1.63	21.73*	8.10	0.03	3.82	27.3	27.3	35.8	2370.0	2217.2	2183.4	331.1	330.6	308.6	25.9	303.6
3-3, 44-46	1072.8	-1.46	21.78*	8.12	0.03	3.55	26.5	26.4	35.8	2369.2	2233.3	2201.3	314.3	313.9	295.3	24.5	290.8
3-3, 51-53	1078.9	-1.23	22.18*	8.17	0.03	3.46	26.2	26.0	36.0	2385.5	2248.6	2216.6	273.9	271.7	257.3	20.7	253.4
3-4, 5-7	1168.3	-1.53	22.09	8.16	0.03	3.45	26.1	26.0	35.9	2381.3	2248.1	2216.7	281.2	279.4	264.5	21.4	260.6
3-4, 40-42	1192.4	-0.95	22.78	8.24	0.02	3.26	25.5	25.1	36.3	2406.1	2271.3	2239.2	222.2	218.3	209.0	16.2	205.8
3-4, 68-70	1212.5	-0.69	22.52	8.22	0.02	3.10	25.0	24.6	36.2	2399.3	2266.4	2234.0	235.1	231.5	221.3	17.3	217.9
3-4, 96-98	1233.3	-1.52	22.26	8.19	0.02	3.31	25.7	25.6	35.8	2370.5	2234.7	2202.6	259.4	258.9	243.6	19.5	239.9
3-4, 103-105	1238.7	-1.59	22.06	8.15	0.03	3.59	26.6	26.5	35.8	2371.8	2235.0	2203.8	287.9	287.3	270.4	22.0	266.4
3-4, 138-140	1253.0	-0.59	22.83	8.24	0.02	2.98	24.5	24.0	36.3	2407.6	2303.7	2271.9	210.3	206.0	200.6	15.4	197.6
3-5, 2-4	1261.7	-1.32	22.37	8.20	0.02	3.29	25.6	25.4	36.1	2389.4	2260.9	2229.8	252.1	249.5	237.7	18.8	234.3
3-6, 3-5	1353.3	-1.61	21.90	8.14	0.03	3.53	26.4	26.3	35.8	2374.1	2240.8	2210.1	301.7	300.7	283.8	23.4	279.7
3-6, 80-82	1412.7	-0.68	22.68	8.23	0.02	3.29	25.6	25.2	36.3	2403.9	2290.5	2260.1	229.9	226.1	218.4	17.0	215.3
4-1, 38-40	1499.2	-0.87	22.23	8.17	0.03	3.49	26.3	25.8	36.4	2412.1	2344.1	2313.8	274.6	269.2	266.4	21.4	262.7
4-1, 66-68	1578.9	-0.87	22.64	8.23	0.02	3.23	25.4	25.1	36.1	2394.3	2247.6	2209.1	229.8	226.9	214.8	16.8	210.9
4-2, 0-2	1653.0	-0.75	22.58	8.23	0.02	3.07	24.9	24.4	36.3	2405.1	2247.9	2207.7	230.3	226.0	214.3	16.7	210.2
4-2, 7-9	1666.8	-0.99	22.55*	8.23	0.02	3.11	25.0	24.7	36.1	2389.9	2255.5	2212.1	231.9	229.4	218.1	17.0	213.6
4-2, 10-12	1673.7	-1.38	21.92	8.16	0.03	3.16	25.2	25.0	36.0	2384.2	2267.9	2223.9	286.1	283.7	271.4	22.1	265.8
4-2, 105-107	1854.2	-1.28	22.05*	8.16	0.03	3.46	26.2	26.0	35.9	2378.7	2241.1	2197.1	284.9	283.4	267.5	21.7	261.9
4-2, 115-117	1863.8	-0.60	22.68*	8.25	0.02	2.96	24.5	24.1	36.2	2399.8	2289.6	2244.0	219.0	215.4	208.3	16.1	203.9
4-3, 25-27	1931.8	-1.78	21.76	8.12	0.03	3.44	26.1	26.0	35.9	2377.2	2259.0	2218.0	313.1	311.6	296.7	24.6	291.0
4-3, 46-48	1946.3	-1.07	23.18*	(8.28)	0.02	3.24	25.4	25.1	36.2	2396.4	2261.6	2212.8	(194.3)	(191.8)	(182.6)	(13.9)	(178.4)
4-3, 49-51	1948.2	-0.66	23.09*	8.27	0.02	3.34	25.8	25.4	36.2	2397.7	2267.4	2217.9	202.7	200.0	190.9	14.6	186.4
4-3, 56-58	1955.8	-0.71	23.06*	8.29	0.02	2.99	24.6	24.3	36.1	2391.8	2269.1	2218.6	194.4	192.0	183.7	14.0	179.3
4-3, 81-83	1979.3	-1.30	21.82*	8.14	0.03	3.22	25.4	25.3	35.8	2370.8	2294.1	2248.8	296.5	295.9	286.4	23.5	280.4
4-3, 116-118	2019.7	-1.31	21.80*	8.15	0.03	3.09	24.9	24.9	35.8	2369.4	2309.8	2259.4	292.5	287.3	280.0	22.8	273.5
4-3, 130-132	2042.2	-1.37	22.83*	(8.24)	0.02	3.46	26.2	26.0	36.0	2383.7	2319.2	2252.1	(221.9)	(206.0)	(202.0)	(15.5)	(195.8)
4-3, 133-135	2048.2	-0.84	22.70*	8.22	0.02	3.48	26.2	26.1	36.0	2383.2	2265.3	2207.3	231.8	249.5	238.2	18.9	231.7

References.

S1. B. Hönisch, N. G. Hemming, *Paleoceanography* **19**, doi:10.1029/2004PA001026 (2004).

S2. H. Spero, L. Lavagnino, M. Schmidt, D. Lea, paper presented at the ICP 8, Biarritz, France, 5-10 September 2004.

S3. K. Klochko, A. J. Kaufman, W. Yao, R. H. Byrne, J. A. Tossell, *Earth and Planetary Science Letters* **248**, 261 (2006).

S4. H. Kakihana, M. Kotaka, S. Satoh, M. Nomura, M. Okamoto, *Bull. Chem. Soc. Japan* **50**, 158 (1977).

S5. S. Reynaud, N. G. Hemming, A. Juillet-Leclerc, J.-P. Gattuso, *Coral Reefs* **23**, 539 (2004).

S6. B. Hönisch *et al.*, *Geochim. Cosmochim. Acta* **68**, 3675 (2004).

S7. A. Sanyal *et al.*, *Paleoceanography* **11**, 513 (1996).

S8. A. Sanyal, J. Bijma, H. J. Spero, D. W. Lea, *Paleoceanography* **16**, 515 (2001).

S9. B. Hönisch, N. G. Hemming, *Earth and Planetary Science Letters* **236**, 305 (2005).

S10. B. Hönisch, N. G. Hemming, B. Loose, *Geochimica et Cosmochimica Acta* **71**, 1636 (2007).

S11. A. G. Dickson, *Deep-Sea Res.* **37**, 755 (1990).

S12. P. S. Dekens, D. W. Lea, D. K. Pak, H. J. Spero, *Geochemistry Geophysics Geosystems* **3**, DOI 10.1029/2001GC000200 (2002).

S13. B. Kisakürek, A. Eisenhauer, F. Böhm, D. Garbe-Schönberg, J. Erez, *Earth and Planetary Science Letters* **273**, 260 (2008).

S14. R. Bintanja, R. S. W. van de Wal, *Nature* **454**, 869 (2008).

S15. A. D. Russell, B. Hönisch, H. J. Spero, D. W. Lea, *Geochim. Cosmochim. Acta* **68**, 4347 (2004).

S16. J. Bijma, B. Hönisch, R. E. Zeebe, *Geochemistry Geophysics Geosystems* **3**, 10.1029/2002GC000388 (2002).

S17. R. Schiebel, S. Barker, R. Lendt, H. Thomas, J. Bollmann, *Deep Sea Research Part II: Topical Studies in Oceanography* **54**, 676 (2007).

S18. G. L. Foster, *Earth and Planetary Science Letters* **271**, 254 (2008).

S19. J. Yu, H. Elderfield, B. Hönisch, *Paleoceanography* **22**, (2007).

S20. P. U. Clark *et al.*, *Quaternary Science Reviews* **25**, 3150 (2006).

S21. B. E. Bemis, H. J. Spero, J. Bijma, D. W. Lea, *Paleoceanography* **13**, 150 (1998).